



**Peer Review** The peer review history for this article is available as a PDF in the Supporting Information.

**Key Points:**

- Rossby wavenumber-5 pattern (wave5) in the jet stream drives summertime compound climate extremes
- The frequency of these summertime wave5 driven extremes has not yet changed due to anthropogenic warming
- Over the last millennium, wave5 related extremes during the summer tend to be preceded by a La Niña winter

**Supporting Information:**

Supporting Information may be found in the online version of this article.

**Correspondence to:**

E. Broadman,  
[ebroadman@arizona.edu](mailto:ebroadman@arizona.edu)

**Citation:**

Broadman, E., Kornhuber, K., Dorado-Liñán, I., Xu, G., & Trouet, V. (2025). A millennium of ENSO influence on jet stream driven summer climate extremes. *AGU Advances*, 6, e2024AV001621. <https://doi.org/10.1029/2024AV001621>

Received 12 DEC 2024

Accepted 20 JUN 2025

**Author Contributions:**

**Conceptualization:** Ellie Broadman, Valérie Trouet

**Data curation:** Ellie Broadman

**Formal analysis:** Ellie Broadman,

Kai Kornhuber, Guobao Xu

**Investigation:** Ellie Broadman,

Kai Kornhuber, Isabel Dorado-Liñán, Valérie Trouet

**Methodology:** Ellie Broadman,

Kai Kornhuber, Isabel Dorado-Liñán, Guobao Xu, Valérie Trouet

**Project administration:** Ellie Broadman, Valérie Trouet

**Resources:** Valérie Trouet


**Supervision:** Valérie Trouet

**Validation:** Ellie Broadman

© 2025. The Author(s).

This is an open access article under the terms of the [Creative Commons Attribution License](#), which permits use, distribution and reproduction in any medium, provided the original work is properly cited.

## A Millennium of ENSO Influence on Jet Stream Driven Summer Climate Extremes

Ellie Broadman<sup>1</sup> , Kai Kornhuber<sup>2,3</sup>, Isabel Dorado-Liñán<sup>4</sup> , Guobao Xu<sup>5</sup>, and Valérie Trouet<sup>1</sup> 

<sup>1</sup>Laboratory of Tree-Ring Research, University of Arizona, Tucson, AZ, USA, <sup>2</sup>International Institute for Applied Systems Analysis, IIASA, Laxenburg, Austria, <sup>3</sup>Lamont Doherty Earth Observatory, Columbia University, New York, NY, USA, <sup>4</sup>Departamento de Sistemas y Recursos Naturales, Universidad Politécnica de Madrid, Madrid, Spain, <sup>5</sup>Shaanxi Key Laboratory of Earth Surface System and Environmental Carrying Capacity, College of Urban and Environmental Sciences, Northwest University, Xi'an, China

**Abstract** Summertime spatially compound climate extremes in the Northern Hemisphere are associated with dominant jet stream Rossby wavenumber patterns, including wavenumber5 (wave5). However, our knowledge of wave5, including its response to anthropogenic warming, is limited by the short length of instrumental records of upper-level fields. To provide a longer-term perspective, we present a 1,000-year reconstruction of a wave5 pattern that modulates summertime compound extremes, constructed by targeting drought anomalies associated with this pattern in three regions. Our results show no major trends in the occurrence of this pattern over the past millennium. We further show that La Niña winters often precede a wave5 event the following summer, evident over centuries. This pattern was exemplified by the La Niña winter of 2022–2023, which was followed by wave5-driven compound heatwaves in July. The imprint of continued anthropogenic warming on ENSO may exacerbate wave5-driven extremes, especially if the tropical Pacific becomes more La Niña-like.

**Plain Language Summary** The jet stream, a band of strong winds high above the Earth's surface, is related to atmospheric patterns that can lead to extreme climate events that occur simultaneously in multiple locations around the Northern Hemisphere during the summer. One such pattern occurs when the jet stream forms five peaks and troughs around the Northern Hemisphere (referred to as a wavenumber-5 pattern, or wave5), resulting in a higher likelihood of co-occurring extreme climate events. We use tree-ring-based data to reconstruct this wave5 pattern during the early summer months over the past millennium and find no major trends in the pattern over this time period. We also find a relationship between this wave5 pattern in the jet stream and the El Niño Southern Oscillation, where anomalously cool sea-surface temperatures in the tropical Pacific (La Niña-like winters) often precede a summer where the jet stream is commonly in a wave5 pattern, driving extreme events.

### 1. Introduction

As the Earth's surface warms under anthropogenic forcing, compound climate extremes are becoming more frequent and intense (AghaKouchak et al., 2020). Of these extremes, concurrent summertime heatwaves and droughts in the Northern Hemisphere are particularly consequential for both ecosystems and human systems. Concurrent heatwaves and droughts have the potential to disrupt multiple important crop-growing regions simultaneously (Gaupp et al., 2020; Kornhuber et al., 2023; Rogers et al., 2022; Sarhadi et al., 2020), which can contribute to global food shortages (Puma et al., 2014; d'Amour et al., 2016) and price spikes. More broadly, extreme heat also drives forest fires (Nojarov & Nikolva, 2022), reduces carbon stocks (Arias-Ortiz et al., 2018), adversely impacts human health (Chen et al., 2024; Florido et al., 2021) and socio-economic systems (Zhou et al., 2024), and drives climate related migrations (Nawrotzki et al., 2016). Indeed, in July 2023 simultaneous record-breaking heatwaves in China, the southwestern United States, and southern Europe demonstrated the threat posed by these compound extremes in a warming world, as heat related deaths and crop failures occurred in each region (World Weather Attribution, 2023). Because spatially compounding climate extremes are influenced by both anthropogenic warming and atmospheric dynamics (Rogers et al., 2022), there is growing interest in understanding changes to the dynamical drivers of these compound extremes (Goddard & Gershunov, 2020; Kornhuber et al., 2020; Wei et al., 2021) as average global temperature continues to rise (IPCC, 2022; Vautard et al., 2023).

**Visualization:** Ellie Broadman  
**Writing – original draft:** Ellie Broadman  
**Writing – review & editing:**  
Ellie Broadman, Kai Kornhuber,  
Isabel Dorado-Liñán, Guobao Xu,  
Valérie Trouet

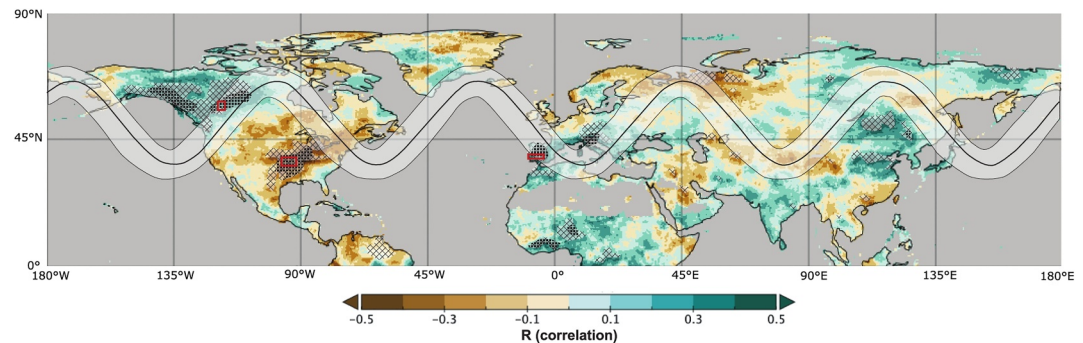


**Figure 1.** Rossby wavenumber-5 pattern and its relationship to self-calibrating Palmer Drought Severity Index (scPDSI) values. The colored map shows the Pearson correlation between the instrumental summer (MJJ) wave5-PC target and scPDSI (<https://crudata.uea.ac.uk/cru/data/drought/>) values from 1948 to 2018 CE. Statistically significant values ( $p \leq 0.1$ ) are stippled, and values that remain significant after applying the false discovery rate (FDR) correction are additionally shaded with black squares. Red boxes show the locations of the three regions used in the multiple linear regression model for the reconstruction. The configuration of Rossby wavenumber-5 in its “preferred” phase (as used to compute wave5-PC) is shown with the black line (median) and gray ribbon (full zonal range of preferred phase).

One important dynamical driver of terrestrial climate extremes in the Northern Hemisphere is the polar jet stream (Screen & Simmonds, 2014). Jet stream winds shift with changes in temperature and pressure at the Earth's surface: the winds intensify and form a tighter ring when latitudinal temperature and pressure gradients are strong, whereas they can slow down when temperature and pressure gradients slacken (Chemke & Coumou, 2024) and can become more sinuous with higher land-ocean temperature gradients (Moon et al., 2022). These shifts in jet stream position and speed impact terrestrial climate by altering spatial patterns and progression of high and low-pressure systems and their hemispheric organization (Brunner et al., 2018; Dong et al., 2013). These surface pressure anomalies can cause simultaneous persistent extreme climate events, such as heatwaves, floods, and wildfires, especially if the jet stream gets stuck in a configuration linked to atmospheric blocking, forming high amplitude ridges and troughs around the Northern Hemisphere (Kornhuber et al., 2019, 2020; Röthlisberger et al., 2016; Rousi et al., 2022; Scholten et al., 2022; Wahl et al., 2019; Xu et al., 2024).

One highly debated topic concerns the waviness of the jet stream under anthropogenic warming. Some studies suggest that the jet stream will become wavier as the globe warms (Coumou et al., 2015; Francis & Vavrus, 2015; Mann et al., 2017; Trouet et al., 2018), while others suggest it will migrate northward (Hallam et al., 2022; Osman et al., 2021), and still others reveal no discernible changes (Barnes & Screen, 2015; Blackport & Screen, 2020; Brönnimann et al., 2025; Kornhuber et al., 2020; Woollings & Blackburn, 2012). It is also uncertain how oceanic and atmospheric modes of variability, such as the El Niño Southern Oscillation (ENSO), may interact with jet stream waviness, especially when modulated by global warming (Cohen, 2016; Di Capua et al., 2021; Wang et al., 2021). For example, the July 2023 compound heatwaves were driven by a stationary, wavey jet stream (World Meteorological Organization, 2023) and were likely intensified by a developing El Niño event in the tropical Pacific Ocean (NOAA Climate Prediction Center, 2023). Insights into jet stream interactions with modes of climate variability inform the debate on drivers of jet stream waviness under anthropogenic warming (Wang et al., 2020; Woollings et al., 2023) and elucidate possible feedbacks between tropical climate and extratropical atmospheric circulation (Alfaro-Sanchez, 2018).

To characterize the waviness of the jet stream, it is useful to consider the dynamics of planetary waves, or Rossby waves (Madden, 2007). One metric used to describe Rossby waves is the zonal wavenumber, named for the number of wave cycles in an atmospheric Rossby wave as it circumvents the Northern Hemisphere (Blackmon & White, 1982), forming a circumglobal teleconnection (Ding & Wang, 2005). Some wavenumber patterns have been related to chains of blocking that drive compound summertime weather extremes in recent decades (e.g., Di Capua et al., 2021; Wicker et al., 2024). Wavenumber 5 (wave5) (Figure 1) and wavenumber 7 (wave7) have repeatedly been associated with major heatwaves, droughts, and floods throughout the Northern Hemisphere due to this phenomenon (Di Capua et al., 2021; Kornhuber et al., 2020) but other wavenumbers within the synoptic scale have been found to be relevant as well (Screen & Simmonds, 2014; Yang et al., 2024). These wavenumbers directly refer to the number of high- and low-pressure systems in the mid-latitudes that are then associated with

often persistent and extreme weather events at the Earth's surface. When the jet stream is in certain wavenumber configurations the wavetrain tends to lock, trapping surface-level pressure systems in stationary locations for days at a time (White et al., 2022).

Compared to most Rossby wavenumbers, a wave5 jet stream pattern is a robust feature of internal climate variability, and its influence on climate extremes has been well documented. For example, wave5 forms a recurrent teleconnection pattern with similar centers of action as the summertime circumglobal teleconnection (CGT) identified by Ding and Wang (2005). Variations in the CGT are associated with climate anomalies across North America, Europe, and Asia (Ding & Wang, 2005), demonstrating the influence of a wave5 jet stream configuration on summer climate in the Northern Hemisphere. The influence of wave5 on summer climate is further evidenced by the numerous climatic extremes in recent decades that have been driven by a wave5 wavetrain (Tables S1 and S2; Figure S1 in Supporting Information S1) (Chang & Wallace, 1987; Di Capua et al., 2021; Grams et al., 2014; Kornhuber et al., 2020; Ulbrich et al., 2003; Zhang et al., 2015). Teleconnections between the CGT and ENSO have also been identified (Ding & Wang, 2005), indicating the potential for relationships between wave5 and oceanic and atmospheric modes of climate variability.

To analyze the dynamics of jet stream wavenumbers and their response to anthropogenic warming, a long-term perspective is needed to provide information on steady state conditions, as instrumental records do not extend prior to the industrial period and atmospheric dynamical variables are notoriously noisy. To this end, we present a novel millennium-length reconstruction (1000–2005 CE) of jet stream waviness using a Rossby wavenumber framework, focusing on the frequency of early Northern Hemisphere summer (May–June–July) wave5 patterns that cause stationary wavetrains and compound climate extremes. We also examine the relationship between the frequency of this wave5 pattern and ENSO, one of the most important modes of variability for driving extreme weather events globally (Rifai et al., 2019). Our results highlight the relationship between tropical sea-surface temperatures and extra-tropical atmospheric circulation, potentially informing efforts to predict weather extremes, and offer insight regarding the evolution of the jet stream under anthropogenic warming.

## 2. Materials and Methods

### 2.1. Wave5-PC Target Index

To reconstruct wave5, we targeted events where the Rossby wavetrain becomes locked in a high amplitude configuration for multiple days. We chose this target because such locked wave5 events should be impactful enough to be recorded in tree-ring proxy indicators, and because they are societally relevant: a high amplitude wavetrain encourages prolonged atmospheric blocking, leading to climate extremes (Kornhuber et al., 2020).

To develop the reconstruction target, we used data derived from a Fourier transform of meridional wind speed at 300 mb in the NCEP/NCAR reanalysis (1948–2018 CE), which gives the dominant phase and amplitude for these winds in each week of the early boreal summer (Kornhuber et al., 2020) (see Data Set S1). These variables are related to wavenumbers as described by the simple fluid dynamics shown in Equation 1:

$$\psi = A \sin(k \lambda - \rho) \quad (1)$$

where  $\psi$  is the wavefunction,  $A$  is the amplitude,  $k$  is the zonal wavenumber,  $\lambda$  is the longitude, and  $\rho$  is the phase (Karoly, 1983).

In Equation 1, amplitude describes the latitudinal extent of the wave, and phase summarizes its longitudinal position around the Northern Hemisphere. For wavenumber patterns that are likely to cause summer climate extremes, like wave5, a locked wavetrain and associated climate anomalies are more likely to occur in certain phases, and during high amplitude events (Kornhuber et al., 2020). In choosing a metric for our reconstruction target, we created an index related to both phase and amplitude, but with an emphasis on phase. This is because high amplitude events can occur in any phase (zonal position), so an index related only to amplitude might not capture blocking and climate extremes occurring in the same locations over time. Kornhuber et al. (2020) showed that wave5 phases between 0 and  $\frac{1}{2}\pi$ , or centered on longitudes of  $0^\circ$ – $90^\circ$ , tend to correspond with high amplitude events, phase-locking, and climate anomalies (Figure 1). Therefore, wave5 phases within this range are an appropriate target for climate reconstruction, capturing both consistency in zonal location and intensity/duration of the high amplitude events that cause climate anomalies of interest. We focused on events that occur during

May, June, and July (MJJ) for our target index, because the high- and low-level meridional wind and pressure anomalies driven by jet stream dynamics change their spatial configuration in August and September compared to June and July (Ding & Wang, 2005).

To produce the target index, we leveraged this relationship between certain wave5 phases, a locked wavetrain, and subsequent climate extremes (Figure 1). Using data from our Fourier transform of 300 mb meridional wind from the NCEP/NCAR reanalysis (Kalnay et al., 1996; Kornhuber et al., 2020), for each year we tallied the number of weeks during MJJ when the average phase for wave5 was centered on longitudes of 0°–90°, the longitudes associated with high amplitude positions that are known to cause anomalous and often impactful weather and climate events. The range of possible values for this metric is 0–13 tallied weeks. We then weighted this value by the number of these preferred phases that co-occur with high amplitude waves ( $\geq 1\sigma$  above average), as measured by procedures described by Kornhuber et al. (2020), giving more weight to years with more events that contain clearly expressed high amplitude events in our targeted zonal position. Specifically, we weigh the initial phase tally (0–13, representing the number of weeks of MJJ dominantly in a preferred phase) by 10% of that phase-tally value for each high amplitude event (see Data Set S1). The scale for our target index exceeds 13, theoretically ranging to 29.9 (if every single week of the 13 weeks in MJJ was dominated by high amplitude conditions). This method accounts only for high amplitude events that exceed our chosen threshold ( $\geq 1\sigma$ ), meaning that lower amplitude values are not registered in our target index.

We termed this index the “wave5 phase count” (wave5-PC), corresponding to our target “wave5-PC” index for the instrumental period (1948–2018 CE). In the wave5-PC index, a higher value represents a summer where the jet stream was more frequently in a wave5 configuration that causes high amplitude events, blocking, and spatially concurrent extreme climate anomalies over the selected regions. This target index expresses the amount of time within a given MJJ season that the wave5 pattern is in a configuration likely to induce a compound extreme event, but does not distinguish whether these event weeks were consecutive. For example, a year with two separate weeks dominated by the preferred phase position and high amplitude would have the same value in our index as a year where these weeks were consecutive. The weekly timescale, as chosen initially by Kornhuber et al. (2020), is appropriate for this analysis because the wave5 “events” of interest occur on the timescale of multiple consecutive days, meaning that a daily timescale would not capture this prolonged nature of the pattern of interest.

To investigate the relationships between the wave5-PC target and climate variables, we computed spatial correlations between the target time series and early summer (MJJ) gridded surface temperature (HadCRU4; <https://www.metoffice.gov.uk/hadobs/hadcrut4/>), precipitation (CRU TS v4.04; [https://crudata.uea.ac.uk/cru/data/hrg/cru\\_ts\\_4.04/](https://crudata.uea.ac.uk/cru/data/hrg/cru_ts_4.04/)), self-calibrating Palmer Drought Severity Index (scPDSI; <https://crudata.uea.ac.uk/cru/data/drought/>), and sea level pressure (SLP; ERA5 reanalysis; <https://www.ecmwf.int/en/forecasts/dataset/ecmwf-reanalysis-v5>) data over the period of overlap between these data sets and the target (1948–2018 CE). We also computed composites for each of these climate variables for the years with the highest (80th percentile; d80; Figure 2) and lowest (20th percentile; d20; Figure S2 in Supporting Information S1) wave5-PC values (Table S1 in Supporting Information S1), to demonstrate that years with high wave5-PC values show climate anomalies associated with a locked wave5 pattern. To mitigate the increase in false positives in these field analyses, we use the Benjamini–Hochberg false discovery rate (FDR) correction for  $P$ -values (Benjamini & Hochberg, 1995). Specifically, we set  $\alpha_{\text{FDR}} = 0.1$  in order to maintain a global  $\alpha$  level of 0.05 (Wilks, 2016).  $P_{\text{FDR}}$  was estimated as follows:

$$P_{\text{FDR}} = \max_{j=1, \dots, k} [P_j : P_j \leq (j/N)\alpha_{\text{FDR}}] \quad (2)$$

where  $\alpha_{\text{FDR}}$  is the control level for FDR,  $P_j$  is the  $P$ -value of the  $j$ th local test after sorting  $P$ -values in an ascending order, and  $N$  is the total number of local tests. Grid cells with  $P$ -values of local test less than  $P_{\text{FDR}}$  are considered significant.

We also computed spatial correlations between the wave5-PC target and 200 mb geopotential height (gph) from the NCEP/NCAR reanalysis over the period of overlap (1948–2018 CE) to compare with the circumglobal teleconnection (CGT) pattern, defined as the second empirical orthogonal function (EOF) of 200 mb gph in the summer (JJAS) months (Ding & Wang, 2005). To do this, we conducted an EOF analysis (Lorenz, 1956) on the



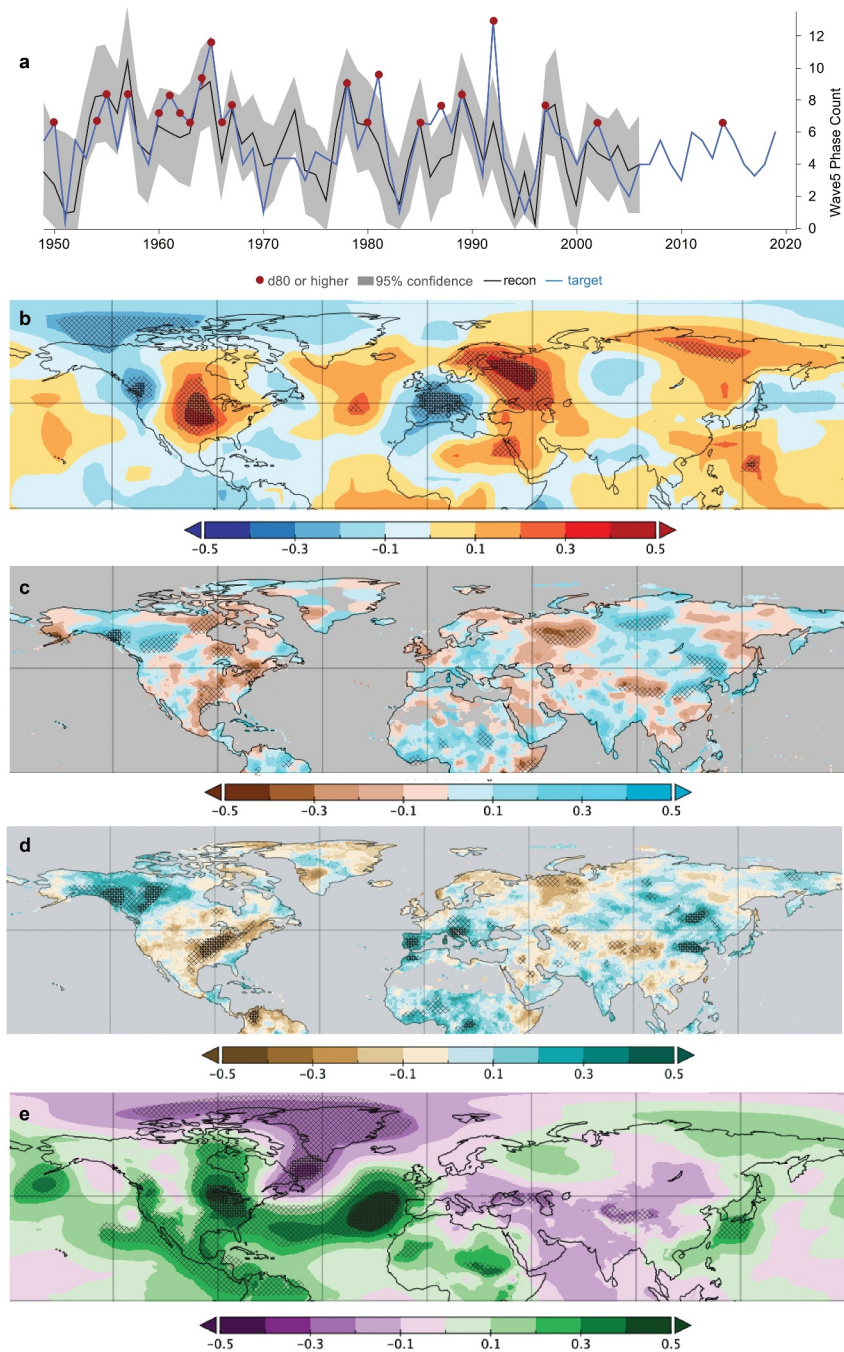


**Figure 2.** Relationships between wave5-PC and summer climate variables. (a) Comparison between reconstructed early boreal summer wave5-PC and instrumental wave5-PC (1948–2005 CE). Red dots show the years corresponding to instrumental wave5-PC values in the 80th percentile (d80), which are first composited and then correlated with climate variables of interest in (b–e). (b) Early summer (MJJ) temperature (HadCRU4; <https://www.metoffice.gov.uk/hadobs/hadcrut4/>) map for years between 1948 and 2018 CE (target time series) with high wave5-PC values (d80). (c) As in (b), but for MJJ precipitation (CRU TS v4.04; [https://crudata.uea.ac.uk/cru/data/hrg/cru\\_ts\\_4.04/](https://crudata.uea.ac.uk/cru/data/hrg/cru_ts_4.04/)). (d) As in (b), but for self-calibrating Palmer Drought Severity Index (scPDSI; <https://crudata.uea.ac.uk/cru/data/drought/>). (e) As in (b), for sea level pressure from 1950 to 2018 CE (<https://www.ecmwf.int/en/forecasts/dataset/ecmwf-reanalysis-v5>; ERA5 reanalysis). In (b–e), statistically significant values ( $p \leq 0.1$ ) are stippled, and values that remain significant after applying the false discovery rate (FDR) correction are additionally shaded with black squares.

200 mb gph field of the NCEP/NCAR reanalysis (Kalnay et al., 1996) from 1948 to 2018 CE, after passing the data through a high-pass filter (11 years). We then computed correlations between the corresponding scores of the second principal component, representing the CGT, and wave5-PC (Figure S3 in Supporting Information S1). Both this correlation and the similar spatial pattern between wave5-PC and the CGT demonstrate that the two are related, despite the differences in seasonality (MJJ vs. JJAS) (Figure S3 in Supporting Information S1).

## 2.2. Wave5-PC Reconstruction

To reconstruct wave5-PC back to 1000 CE, we leveraged the correlation between our target index and scPDSI (Figure 1; Figure S4 in Supporting Information S1) as recorded in tree-ring data. Because our reconstruction targets a specific spatial pattern in surface climate conditions, as driven by a particular wave5 position (phase), tree-ring data are well suited for our approach: the regions that are impacted by our targeted wave5 events will be the same each time this pattern occurs, because it is zonally constrained. Therefore, the same trees will experience the same wave5-driven climate impacts each time the pattern occurs. Spatial correlations with temperature over the instrumental period are robust in several regions (Figure 2b; Figure S4a in Supporting Information S1), but the slight seasonal offset between the sensitivity of most summer temperature tree-ring proxies (e.g., maximum latewood density) and our target time series resulted in difficulties finding statistically significant temporal correlations between wave5-PC and tree-ring-derived temperature reconstructions.

Instead of temperature, we pursued our reconstruction using tree-ring derived scPDSI data. Our target season works well for scPDSI data, because MJJ is the time of year in which numerous tree species are most hydroclimatically sensitive (e.g., Stambaugh et al., 2011; Touchan et al., 2017), meaning that we are more likely to capture hydroclimatic variability related to wave5 during this early summer season. scPDSI (“self-calibrating” PDSI) differs from standard PDSI because values are adjusted to local historical climate data, yielding values that are more consistent and comparable across regions, especially at the global scale (Wells et al., 2004). As such, scPDSI is particularly well suited to our global-scale reconstruction of wave5-PC, which relies upon the relationship between wave5-PC and scPDSI from two locations in North America and one location in Europe as recorded in the North American Drought Atlas (NADA) and the Old World Drought Atlas (OWDA). These gridded ( $0.5^\circ \times 0.5^\circ$ ) products contain gridded summer (JJA) scPDSI reconstructions based on a large network of moisture-sensitive tree-ring chronologies, derived by spatially interpolating moisture-sensitive tree-ring data over the last several hundred to 2,000 years, depending on the location. As such, they offer an opportunity to use spatially reconstructed, tree-ring-derived scPDSI data even in locations where not many moisture-sensitive tree-ring chronologies are available (e.g., in the central plains of the United States). Because scPDSI is a time-integrated variable, conditions in MJJ (represented by wave5-PC due to changing jet stream conditions in August) should be well represented by the JJA scPDSI values derived from the drought atlases, as evidenced in part by correlations between wave5-PC (MJJ) and scPDSI (JJA) over the instrumental period (Figure 2d). The approach of using gridded climate data as the target(s) for a tree-ring based reconstruction has been employed in several previous studies (e.g., Graham & Hughes, 2007; Nguyen & Galelli, 2018). We derived three scPDSI time series from two locations in North America (NADA) and one location in Europe (OWDA) where scPDSI is strongly correlated with the wave5 target from 1948 to 2018 CE (Figure 1; Table S2; Figure S5 in Supporting Information S1). Each time series extends back to 1000 CE (Figure S6 in Supporting Information S1). In the drought atlases, each  $0.5 \times 0.5$  grid cell incorporates information from a minimum of 20 tree-ring chronologies within a 1,000–1,500 km radius (Cook et al., 2015); as such, there are >20 chronologies incorporated into each of our three scPDSI time series (Cook et al., 2007, 2015). We used each of these three time series as predictors (independent variables) in a multiple linear regression (MLR) model, with wave5-PC as the reconstruction target (dependent variable).

To evaluate the MLR model, we used the adjusted R-squared ( $R^2_{adj}$ ), an  $F$ -test, and Akaike information criterion (AIC) parameters. We also evaluated reconstruction skill based on reduction of error (RE), coefficient of efficiency (CE) (Cook & Kairiukstis, 1990), and  $R^2_{adj}$  over two periods of equal length (split period calibration) covering the common period between our reanalysis-based target and the chronologies (1948–1975 CE and 1976–2005 CE) (Table S3 in Supporting Information S1). We then scaled the reconstruction to fit the mean and variance of the wave5-PC target over the overlap period (1948–2005 CE) (Esper et al., 2005). We chose this standard scaling method because it performed more successfully (i.e., reconstructed values more closely matching the target) compared to quantile scaling (Robeson et al., 2020). We estimated uncertainty in the reconstruction based on the calibration uncertainty (Esper et al., 2007) using the root mean square error ( $\pm 1$  RMSE) derived from the

MLR of the reconstruction against the target. We further calculated correlation coefficients between the reconstructed and instrumental wave5-PC target at high and low frequencies using 20-year spline high-pass and low-pass filters, respectively (Figures S7a and S7b in Supporting Information S1). We also conducted a cross-wavelet coherency analysis (Torrence & Compo, 1998) between instrumental and reconstructed wave5-PC to evaluate coherence in their variability (Figure S7c in Supporting Information S1).

Quantifying certain sources of uncertainty (“detrending error” and “chronology error” per Esper et al., 2007) in a reconstruction based on drought atlas data is challenging, because NADA and OWDA are regression products with inherent uncertainties that increase as the number of available chronologies decreases back in time. These uncertainties are not represented by the drought atlas data used as the inputs to our reconstruction model. However, a major advantage of this approach is that the tree-ring chronologies used in NADA and OWDA are already detrended and standardized. In our reconstruction we do estimate uncertainty in the reconstruction using bootstrapping, as described by Nguyen et al. (2020). Specifically, using the *R* package “boot”, we ran our reconstruction model using our three drought-atlas-derived time series 10,000 times, and then calculated the lower and upper 95% confidence intervals for the reconstruction based on those 10,000 iterations. These estimates constitute the “reconstruction error” (per Esper et al., 2007) for this time series. We further quantify the “calibration error” (per Esper et al., 2007) by applying the residual standard error of our model as additional upper and lower bounds for the reconstructed values.

### 2.3. Comparison With the El Niño Southern Oscillation

To analyze the relationship between wave5-PC and ENSO, we first calculated Pearson correlations over the period of overlap with both instrumental and reconstructed ENSO time series. Instrumental sea surface temperature anomaly (SSTA) data for the Niño 3, Niño 3.4, Niño 4, and Multivariate ENSO (MEI) indices were taken from the NOAA Physical Science Laboratory (<https://psl.noaa.gov/data/gridded/data.noaa.ersst.v5.html>). We then computed Pearson correlations between these indices and wave5-PC for 1854–2018 CE, the period for which we have both wave5-PC data and instrumental SSTA data. As part of this analysis, a correction for autocorrelation was performed (Bretherton et al., 1999). We also computed the spatial correlation between wave5-PC over this interval and SSTAs using the HadISST1 data set ( $1^\circ \times 1^\circ$ ; <https://hadleyserver.metoffice.gov.uk/hadisst/>) in the KNMI Climate Explorer (<https://climexp.knmi.nl/>). We also conducted a boxplot analysis for the ENSO time series and the wave5-PC index, comparing the values in one boreal winter (DJF) of the ENSO time series to the following boreal early summer for wave5-PC.

To evaluate whether extreme wave5-PC values are associated with SSTA's in the ENSO indices, we then conducted a bootstrap superposed epoch analysis (SEA) (Haurwitz & Brier, 1981) using the wave5-PC index from 1854 to 2018 CE as the continuous time series. We considered the 90th percentile (d90) and 10th percentile (d10) of the Niño 3, Niño 3.4, and Niño 4 indices, as well as El Niño and La Niña events in the multivariate ENSO index (MEI), as event years in the SEA. We superposed an 11-year window (5 years before and 5 years following) to analyze contemporaneous and lagged relationships from 1854 to 2018 CE. We defined anomalies in the continuous wave5-PC time series with respect to the mean over the 5-year period preceding a wave5-PC event, which can minimize the effect of low-frequency variability on the analysis (Rao et al., 2019). Monte Carlo simulations ( $n = 10,000$ ) were applied to develop bootstrapped 95% confidence intervals (Rao et al., 2019).

To analyze these relationships in the past, we conducted the same analysis, but using ENSO paleoclimate reconstructions to identify the events for the SEA. For each of these analyses, we similarly used the wave5-PC reconstruction as the continuous time series and computed the d90 and d10 values for the ENSO reconstructions over the period of overlap with the wave5-PC reconstruction, for the following time periods: 1190–2005 CE (Liu et al., 2017), 1617–2005 CE (Freund et al., 2019), and 1301–2005 CE (Li et al., 2013). For the data provided by Gergis and Fowler (2009), which spans 1525–2002 CE, we used reconstructed events classified as “high”, “very high”, or “extreme” as the ENSO event years. Although Li et al. (2013) is based on tree-ring-width proxy data in the drought atlases, the chronologies used for their ENSO reconstruction are independent from those used in our wave5-PC reconstruction; there is no spatial overlap in the regions of focus for the two studies, as Li et al. (2013) focuses on the southwestern United States (in NADA) and data from the Monsoon Asia Drought Atlas.

We also computed all SEAs described above using the opposite data as continuous time series and event years (i.e., using the SSTA's as the continuous time series and extreme (d90 and d10) wave5-PC years as the events),

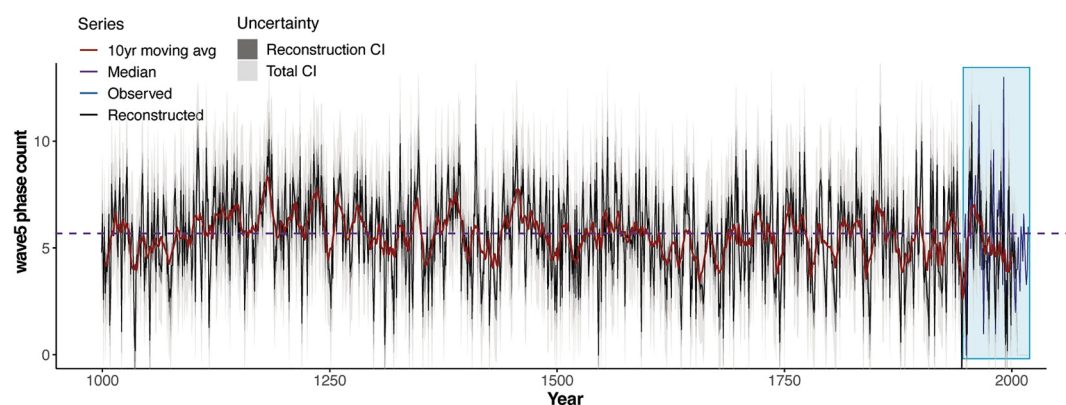


**Figure 3.** Reconstructed wave5-PC from 1000–2005 CE. The black line shows the reconstruction values, with 95% confidence bands associated with calibration uncertainty in dark gray and 95% confidence intervals based on reconstruction uncertainty shown in light gray (see Methods). The period of overlap (1948–2005 CE) with the target (1948–2018 CE; enlarged in Figure 2a) is also shown, with the wave5-PC target in blue. The horizontal dashed line shows the median value of the reconstruction time series, and the red line shows the 10-year running average of the reconstruction.

yielding results with similar patterns in most instances (Figure S8 in Supporting Information S1), though the results are difficult to compare directly because the winter SSTA occurs in a different calendar year (previous winter) compared to the wave5-PC anomaly. Cross-wavelet coherency analysis (Torrence & Compo, 1998) between the SSTA time series and the wave5-PC reconstruction further indicates the coherence in the variability between these data sets (Figure S9 in Supporting Information S1).

### 3. Results

#### 3.1. Wave5-PC Target Index

High wave5-PC values (Figure 2a; Table S1 in Supporting Information S1) over the instrumental period are associated with documented extreme climate events (Table S4, Figure S1 in Supporting Information S1), and with spatially coherent climate anomalies in the Northern Hemisphere, as revealed by temperature, precipitation, and self-calibrating Palmer Drought Severity Index (scPDSI) composites for these summers (Figures 2b–2d). Composited sea level pressure data for these extreme wave5-PC summers also reveal a spatial pattern showing the expected high and low pressure systems commonly related to the climate anomalies targeted in our reconstruction (Figure 2e). These indicators demonstrate that our target index is representative of the climate patterns associated with a locked wave5 wavetrain in this zonal position. Additionally, the correlation between wave5-PC and 200 mb geopotential height (gph) resembles that of the summertime CGT, which is computed as the second EOF of the 200 mb gph field (NOAA Climate Prediction Center, 2023) (Figure S3 in Supporting Information S1; see Methods). Wave5-PC is also moderately positively correlated with the corresponding scores of the second principal component (PC2) of 200 mb gph from 1948 to 2018 CE, which represents the CGT as a time series (Figure S3 in Supporting Information S1; see Methods).

#### 3.2. Wave5-PC Reconstruction

The MLR model that uses our three selected scPDSI time series to predict wave5-PC explains 39% of the variability in the wave5-PC target over the instrumental period, with robust calibration and verification statistics (Table S3 in Supporting Information S1). The variance inflation factor (VIF) for the model is modest (below 2 in all cases), indicating that multicollinearity is not a factor substantially influencing the efficacy of our reconstruction. Using this MLR model, we reconstructed millennium-length (1000–2005 CE) MJJ wave5-PC variability (Figure 3). Our calibration and verification trials show that wave5-PC can be skillfully reconstructed back to 1000 CE (1000–2005 CE), with 40%–42% of the variance explained in the verification procedure and positive RE and CE values. The residuals from the model output expressed a normal distribution, show no trend, and are homoscedastic (Figure S10 in Supporting Information S1), with no outliers detected using Cook's distance index. The calibration and reconstruction error estimates (see Methods) are shown in Figure 3.



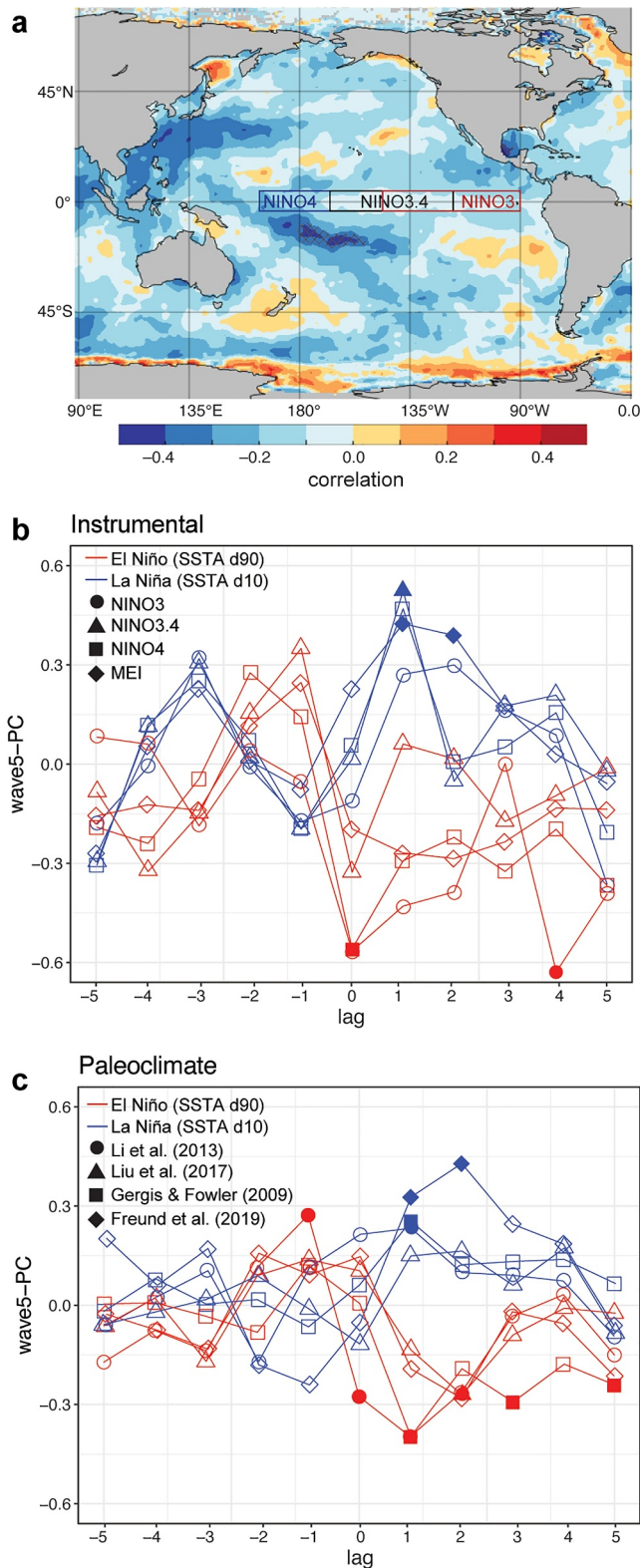


Figure 4.

Because we applied a linear regression to a bounded dependent variable, the resulting reconstruction may occasionally fall outside the theoretical bounds of possible values, specifically by yielding negative values that are unrealistic for a weighted tally of weeks per year. These occurrences are infrequent, affecting <0.1% of values for the median, 1.6% of the lower 95% bootstrapped confidence interval, and in 9.4% of the lower bound of the total reconstruction uncertainty. We simply truncate the lower bound of our reconstruction at zero, as any negative values produced by the linear regression are interpreted to represent 0 weeks with likely wave5 events.

### 3.3. Wave5 and the El Niño Southern Oscillation

The most consistent and prominent relationships between summer wave5-PC and Sea Surface Temperature Anomalies (SSTAs) are during the winter (DJF) preceding a wave5-PC event for the Niño 3, Niño 3.4, Niño 4, and multivariate ENSO (MEI) indices (<https://psl.noaa.gov/data/gridded/data.noaa.ersst.v5.html>). Early summer (MJJ) wave5-PC bears similarity to these winter ENSO indices over the period of overlap with the SSTA data (1854–2018 CE) (see Methods) (Figures S11 and S12 in Supporting Information S1), and the spatial correlation between MJJ wave5-PC and DJF SSTAs over this interval also reveals a pattern reminiscent of a La Niña event (Figure 4a). We further evaluated relationships over the instrumental period using superposed epoch analysis (SEA; see Methods) (Table S5 in Supporting Information S1), which reveals significant departures in wave5-PC during the year following La Niña (anomalously low SSTs) or El Niño (anomalously high SSTs) events (Figure 4b). The results of the SEA using winter (DJF) and spring (MAM) ENSO reconstructions based on various annually resolved proxy data (Freund et al., 2019; Gergis & Fowler, 2009; Li et al., 2013; Liu et al., 2017) (Figure 4c; Table S5 in Supporting Information S1) indicate that this relationship between wave5-PC and ENSO has persisted over the past millennium and is a consistent feature of natural climate variability.

## 4. Discussion and Conclusions

### 4.1. Reconstructed Early Summer Wave5 Events Over the Past Millennium

Our reconstruction reveals that the occurrence of locked, high amplitude wave5 events has remained steady over the past millennium, with some centuries exhibiting more pronounced multi-decadal fluctuations in wave5-

**Figure 4.** Relationship between early boreal summer wave5-PC and winter El Niño Southern Oscillation (ENSO) conditions. (a) The spatial correlation between winter (DJF) sea surface temperature anomalies (SSTA) (HadISST1,  $1^\circ \times 1^\circ$ ; <https://hadleyserver.metoffice.gov.uk/hadisst/>) and the following summer (MJJ) wave5-PC values from 1870 to 2018 CE. Areas with statistically significant values ( $p \leq 0.1$ ) are stippled. (b) Results from a superposed epoch analysis (SEA) of extreme wave5-PC years and instrumental SSTs timeseries for Niño3, Niño3.4, Niño4, and the multivariate ENSO index (MEI) (<https://psl.noaa.gov/data/gridded/data.noaa.ersst.v5.html>) from 1854 to 2018 CE. The x-axis indicates the lag (in years) in the response of wave5-PC to ENSO. (c) As in (b), but for annually resolved proxy-based reconstructions of ENSO indices, including those from tree ring  $\delta^{18}\text{O}$  in Taiwan [56], Pacific corals [57], compiled tree ring widths [58], and a multi-proxy compilation [59]. For (b, c), shapes are filled if values are statistically significant ( $p \leq 0.05$ ). Seasonality of the ENSO proxies is detailed in Table S5 of Supporting Information S1.

PC values (Figure 3; Figure S13 in Supporting Information S1). Both linear and quantile regressions (Khan et al., 2022; Maxwell et al., 2021) that tested for changes in median and extreme values (e.g., d95, d99) over time yielded small slopes ( $m < \pm 0.001$ ), most of which were statistically insignificant. The uncertainties in our reconstruction (Figure 3; Table S3 in Supporting Information S1) and the challenges associated with reconstructing the jet stream, which influences terrestrial surface climate from the top of the troposphere, should be kept in mind in our interpretations of this reconstruction. The period corresponding to the Medieval Climate Anomaly (MCA; 1000–1300 CE) is characterized by slightly higher wave5-PC values ( $\mu = 5.8 \pm 1.3$ ) compared to the period corresponding to the Little Ice Age (LIA; 1300–1850 CE) ( $\mu = 5.5 \pm 1.4$ ) (Figure 3). This could imply that during the MCA, a frequent wave5 pattern might have contributed to more persistent early summer heat waves and droughts in Scandinavia, the British Isles, and much of the continental United States, and cooler and wetter conditions in the Iberian Peninsula and much of Canada (Figures 2b–2d), with the opposite pattern during the LIA. Such a pattern, albeit with substantial temporal and spatial heterogeneity, has previously been documented for MCA and LIA climate in the Iberian Peninsula (Abrantes et al., 2017) and Scandinavia (Björklund et al., 2023; Esper et al., 2014) and is also reminiscent of a summertime dipole in the modern climate of Europe (Dorado-Liñán et al., 2022) and the midwestern United States (Singh et al., 2023). A high frequency of the wave5 pattern during the MCA, a period postulated to be dominated by La Niña-like conditions (Graham et al., 2007; Seager et al., 2007; Trouet et al., 2009), further corresponds to the relationship we find between wave5 and ENSO.

Notably, recent (1948–2018 CE) wave5-PC values are well within the bounds of natural variability as indicated by the millennium-length reconstruction (Figures 2a and 3). In fact, there are periods in the past with substantially higher values than those recorded in recent decades. For example, during the 12th and 13th centuries, wave5-PC values were generally elevated, and in the mid-15th century for ~30 years there was an abrupt shift to some of the highest values in the reconstruction (Figure 3). Furthermore, there is no discernible trend in wave5-PC values over recent decades (Figures 2a and 3). Our findings are supported by an ensemble of monthly and daily atmospheric field reconstructions over Europe showing that recent jet indices fall within variability over the past 600 years (Brönnimann et al., 2025) and indicate that the wave5-PC events targeted for this reconstruction have not become more frequent over the past century. However, the natural variability of wave5-PC, including several intervals with higher values, indicates that a future multi-decadal or multi-centennial period characterized by more frequent wave5-PC events cannot be excluded. In the event of a shift to higher wave5-PC values, the resulting spatially compound climate extremes are likely to be unprecedented in the last millennium context due to the progression of anthropogenic warming and associated feedbacks, which have played a role in recent severe heat extremes (Bartusek et al., 2021; Vautard et al., 2023).

#### 4.2. Wave5 and La Niña

Climate warming is thought to modulate aspects of both the jet stream and ENSO (Cai et al., 2023; Freund et al., 2019; Moon et al., 2022) and both are responsible for terrestrial climate extremes (Cordero et al., 2024; Kornhuber et al., 2020; Rifai et al., 2019). Furthermore, the established relationship between ENSO and the summertime circumglobal teleconnection (CGT) (Ding & Wang, 2005) suggests a possible teleconnection between ENSO and wave5-PC. Our reconstruction results support a millennium-scale teleconnection between these two components of ocean-atmospheric circulation, but the paleoclimate record explains 39% of the variance in wave5-PC (leaving 61% unexplained). Mindfulness of the uncertainties inherent to these paleo results is therefore warranted, but our confidence in the relationship between the two phenomena during the instrumental period is unaffected by these uncertainties, especially given the documented relationship between the two in the existing literature (Di Capua et al., 2021; Ding et al., 2011; Ding & Wang, 2005; Lin et al., 2023; Luo & Lau, 2020; Wang et al., 2012; Yasui & Watanabe, 2010).

The relationship between wave5-PC and tropical Pacific SSTAs, with preceding winter La Niña conditions associated with a wave5 pattern in the boreal summer, is similar to that documented in previous studies focused on the relationship between ENSO and either a wave5 wavetrain or the CGT. For example, Ding and Wang (2005) found La Niña conditions associated with a CGT pattern in the summer (JJAS) and Di Capua et al. (2021) demonstrated that La Niña conditions were associated with extreme events caused by wave5 in the summer of 2010. Proposed mechanisms for this relationship between ENSO and the CGT and/or wave5 include SSTA-driven geopotential height and anticyclonic wind anomalies (Lin et al., 2023; Luo & Lau, 2020; Yasui & Watanabe, 2010) and SSTA-driven modulation of the Indian and Pacific monsoons (Ding et al., 2011; Wang et al., 2012).

Most studies that demonstrate this relationship between ENSO and the CGT find that the relevant SSTAs occur in the spring or summer of a developing La Niña event, during the same season as the wave5 jet stream pattern. Our results suggest the influence of La Niña on wave5 may begin in the previous winter, possibly providing some early predictive power to compound extreme forecasts. This seasonally earlier influence of tropical Pacific SSTAs on the CGT has been previously identified in experiments performed using the Community Earth System Model (CESM) (Lin et al., 2023). Anecdotal evidence for this relationship also occurred in 2023, when concurrent heatwaves in July in the Northern Hemisphere were driven by a wave5 pattern (Figure S14 in Supporting Information S1), with a La Niña event having occurred during the previous winter (DJF 2022–2023 SSTA =  $-1.1^{\circ}\text{C}$ ).

### 4.3. Implications for Future Wave5 and ENSO Behavior

Our millennium-length reconstruction of wave5-PC reveals that the phase locking behavior driving high amplitude early boreal summer wave5 events has consistent multi-decadal natural variability, and, so far, does not exhibit an increasing trend under observed anthropogenic warming. The few other studies that have analyzed trends in summer wave5 behavior report mixed results, with some describing an increase in wave5 events (Lee et al., 2017) and others reporting no statistically significant trend (Kornhuber et al., 2020). Based on reanalysis data as well as CMIP6 baseline simulations, Teng et al. (2022) recently suggested that a related jet stream pattern is modulated by Atlantic multidecadal variability and might have become more frequent in response to anthropogenic climate change. This pattern shows a compound warming signal over the Atlantic, Eastern Europe, and the western United States that is similar to the footprint of the wave5 pattern. Our finding that the occurrence of summer wave5 events shows no significant trend in the Industrial Era underscores the need for data sets that extend beyond the instrumental period to evaluate recent wave5 variability against baseline conditions. This supports previous research suggesting that the increased frequency of Northern Hemisphere heatwaves associated with wave5 is primarily driven by anthropogenic warming rather than changes in atmospheric circulation (Rogers et al., 2022). This finding, however, does not rule out potential future changes in wave5-PC, nor changes in other characteristics of Northern Hemisphere summertime circulation, such as persistence (Pfleiderer et al., 2019; Teng et al., 2022) and position (Osman et al., 2021) of wave patterns. This result could also suggest that changes in land-ocean temperature contrasts linked to global warming have not yet sufficiently influenced the stationary forcing patterns associated with coastlines or orography (Jiménez-Esteve et al., 2022) to significantly increase the waves' tendencies to lock in specific spatial patterns, though this might occur once the forcing becomes sufficiently strong.

Though intriguing, our findings neither corroborate nor disprove the theory that anthropogenic warming enhances jet stream waviness (Moon et al., 2022). As we have focused on one specific pattern only, the analysis does not allow for broader conclusions on how velocity, location, or waviness have been altered by anthropogenic influences and how these characteristics might evolve in the future. To comprehensively evaluate the impact of relevant characteristics of the jet stream across multiple spatial and temporal scales, more research focused on other seasons, configurations, and measures of jet stream behavior over the past centuries to millennia is needed (Brönnimann et al., 2025; Hu et al., 2022a, 2022b; Osman et al., 2021; Wahl et al., 2019; Xu et al., 2024).

However, we reveal that over the past millennium, La Niña events tend to precede summers with wave5-driven climate extremes, demonstrating the influence of tropical climate on jet stream variability. This finding has the potential to increase long-term predictability of high-impact climate extremes that are typically predicted only days or weeks in advance, which is one of the major challenges of seasonal forecasting (Vitart, 2019). Furthermore, this relationship between ENSO and wave5 means that, as global temperature continues to rise (Peters et al., 2013), related shifts both in the mean state of the tropical Pacific and in the intensity of ENSO events will have implications for summer climate extremes driven by wave5. If the tropical Pacific mean state follows the trend of recent decades and becomes more La Niña-like (Sobel et al., 2023), we may experience more frequent summer climate extremes related to wave5 in future decades, though predictions of future ENSO conditions are uncertain (Seager et al., 2022; Willis et al., 2022). Similarly, with ENSO events projected to become more intense (Cai et al., 2023; Collins et al., 2010), the impact of a naturally occurring period of more frequent wave5 events could have more disruptive consequences (e.g., Kornhuber et al., 2020). As such, our findings demonstrate that robust extreme weather forecasts rely on disentangling the complex interplay between multiple components of variability in the internal climate system and anthropogenic forcing.

## Conflict of Interest

The authors declare no conflicts of interest relevant to this study.

## Data Availability Statement

The instrumental and reconstructed wave5-PC data sets, as well as the NCEP/NCAR wave5 data used in this analysis, are available at the NOAA Paleoclimatology website at <https://www.ncei.noaa.gov/access/paleo-search/study/42679>, and are contained in the attached Data Set S1 file. The NADA and OWDA data sets can be found at <https://www.ncei.noaa.gov/> (Cook et al., 2007, 2015). All instrumental climatological data used in our analyses can be found using the links provided below (also cited in the Main Text):

- HadCRUT4: <https://www.metoffice.gov.uk/hadobs/hadcrut4/> (Morice et al., 2012)
- CRU TS v 4.04: [https://crudata.uea.ac.uk/cru/data/hrg/cru\\_ts\\_4.04/](https://crudata.uea.ac.uk/cru/data/hrg/cru_ts_4.04/) (Harris et al., 2020)
- CRU scPDSI: <https://crudata.uea.ac.uk/cru/data/drought/> (van der Schrier et al., 2013)
- ERA5 Reanalysis: <https://www.ecmwf.int/en/forecasts/dataset/ecmwf-reanalysis-v5> (Hersbach et al., 2020)
- NOAA Extended Reconstructed SST V5: <https://psl.noaa.gov/data/gridded/data.noaa.ersst.v5.html> (Huang et al., 2017)
- HadISST: <https://www.metoffice.gov.uk/hadobs/hadisst/> (Rayner et al., 2003)

The KNMI Climate Explorer can be found at <https://climexp.knmi.nl/start.cgi> (Trouet & Van Oldenborgh, 2013).

## Acknowledgments

We thank Diana Zamora-Reyes and Matthew Meko for their comments and insights that improved this manuscript. This study was supported by the US National Science Foundation (NSF) CAREER Grant AGS-1349942 to VT, by the German Federal Ministry of Education and Research within the ClimXtreme project subproject PERSEVERE (01LP2322D) to KK, and by funding from Proyectos de Generación de Conocimiento, Ministerio de Ciencia e Innovación (#PID2021-128759OA-I00), Ayudas para Incentivar la Consolidación Investigadora (#CNS2022-135228), and Jose Castillejo Mobility Grant 2021 (#CAS21/00210) to IDL.

## References

- Abrantes, F., Rodrigues, T., Rufino, M., Salgueiro, E., Oliveira, D., Gomes, S., et al. (2017). The climate of the common era off the Iberian peninsula. *Climate of the Past*, 13(12), 1901–1918. <https://doi.org/10.5194/cp-13-1901-2017>
- AghaKouchak, A., Chiang, F., Huning, L. S., Love, C. A., Mallakpour, I., Mazdiyasni, O., et al. (2020). Climate extremes and compound hazards in a warming world. *Annual Review of Earth and Planetary Sciences*, 48(1), 519–548. <https://doi.org/10.1146/annurev-earth-071719-055228>
- Alfaro-Sanchez, R., Nguyen, H., Klesse, S., Hudson, A., Belmecheri, S., Köse, N., et al. (2018). Climatic and volcanic forcing of tropical belt northern boundary over the past 800 years. *Nature Geoscience*, 11(12), 933–938. <https://doi.org/10.1038/s41561-018-0242-1>
- Arias-Ortiz, A., Serrano, O., Masqué, P., Lavery, P. S., Mueller, U., Kendrick, G. A., et al. (2018). A marine heatwave drives massive losses from the world's largest seagrass carbon stocks. *Nature Climate Change*, 8(4), 338–344. <https://doi.org/10.1038/s41558-018-0096-y>
- Barnes, E. A., & Screen, J. A. (2015). The impact of Arctic warming on the midlatitude jet-stream: Can it? Has it? Will it? *Interdisciplinary Reviews of Climate Change*, 6(3), 277–286. <https://doi.org/10.1002/wcc.337>
- Bartusek, S., Kornhuber, K., & Ting, M. (2021). North American heatwave amplified by climate change-driven nonlinear interactions. *Nature Climate Change*, 12, 1143–1150. <https://doi.org/10.1038/s41558-022-01520-4>
- Benjamini, Y., & Hochberg, Y. (1995). Controlling the false discovery rate: A practical and powerful approach to multiple testing. *Journal of the Royal Statistical Society: Series B*, 57(1), 289–300. <https://doi.org/10.1111/j.2517-6161.1995.tb02031.x>
- Björklund, J., Seftigen, K., Stoffel, M., Fonti, M. V., Kottlow, S., Frank, D. C., et al. (2023). Fennoscandian tree-ring anatomy shows a warmer modern than medieval climate. *Nature*, 620(7972), 97–103. <https://doi.org/10.1038/s41586-023-06176-4>
- Blackmon, M. L., & White, G. H. (1982). Zonal wavenumber characteristics of Northern Hemisphere transient eddies. *Journal of the Atmospheric Sciences*, 39(9), 1985–1998. [https://doi.org/10.1175/1520-0469\(1982\)039<1985:ZWCONH>2.0.CO;2](https://doi.org/10.1175/1520-0469(1982)039<1985:ZWCONH>2.0.CO;2)
- Blackport, R., & Screen, J. A. (2020). Insignificant effect of Arctic amplification on the amplitude of midlatitude atmospheric waves. *Science Advances*, 6(8), eaay2880. <https://doi.org/10.1126/sciadv.aay2880>
- Bretherton, C. S., Widmann, M., Dymnikov, V. P., Wallace, J. M., & Bladé, I. (1999). The effective number of spatial degrees of freedom of a time-varying field. *Journal of Climate*, 12(7), 1990–2009. [https://doi.org/10.1175/1520-0442\(1999\)012<1990:TENOSD>2.0.CO;2](https://doi.org/10.1175/1520-0442(1999)012<1990:TENOSD>2.0.CO;2)
- Brönnimann, S., Franke, J., Valler, V., Hand, R., Samakinwa, E., Lundstad, E., et al. (2025). Past hydroclimate extremes in Europe driven by Atlantic jet stream and recurrent weather patterns. *Nature Geoscience*, 18(3), 246–253. <https://doi.org/10.1038/s41561-025-01654-y>
- Brunner, L., Schaller, N., Anstey, J., Sillmann, J., & Steiner, A. K. (2018). Dependence of present and future European temperature extremes on the location of atmospheric blocking. *Geophysical Research Letters*, 45(12), 6311–6320. <https://doi.org/10.1029/2018GL077837>
- Cai, W., Ng, B., Geng, T., Jia, F., Wu, L., Wang, G., et al. (2023). Anthropogenic impacts on twentieth-century ENSO variability changes. *Nature Reviews Earth & Environment*, 4(6), 407–418. <https://doi.org/10.1038/s43017-023-00427-8>
- Chang, F.-C., & Wallace, J. M. (1987). Meteorological conditions during heat waves and droughts in the United States Great Plains. *Monthly Weather Review*, 115(7), 1253–1269. [https://doi.org/10.1175/1520-0493\(1987\)115<1253:MCDHWA>2.0.CO;2](https://doi.org/10.1175/1520-0493(1987)115<1253:MCDHWA>2.0.CO;2)
- Chemke, R., & Coumou, D. (2024). Human influence on the recent weakening of storm tracks in boreal summer. *npj Climate and Atmospheric Science*, 7(1), 86. <https://doi.org/10.1038/s41612-024-00640-2>
- Chen, C., Schwarz, L., Rosenthal, N., Marlier, M. E., & Benmarhnia, T. (2024). Exploring spatial heterogeneity in synergistic effects of compound climate hazards: Extreme heat and wildfire smoke on cardiorespiratory hospitalizations in California. *Science Advances*, 10(5), ead7264. <https://doi.org/10.1126/sciadv.ad7264>
- Cohen, J. (2016). An observational analysis: Tropical relative to Arctic influence on midlatitude weather in the era of Arctic amplification. *Geophysical Research Letters*, 43(10), 5287–5294. <https://doi.org/10.1002/2016GL069102>
- Collins, M., An, S.-I., Cai, W., Ganachaud, A., Guilyardi, E., Jin, F.-F., et al. (2010). The impact of global warming on the tropical Pacific Ocean and El Niño. *Nature Geoscience*, 3(6), 391–397. <https://doi.org/10.1038/ngeo868>
- Cook, E. R., & Kairiukstis, L. A. (1990). *Methods of dendrochronology. Applications in the environmental sciences. International Institute for applied systems analysis.* Kluwer Academic Publishers. 394.
- Cook, E. R., Seager, R., Cane, M. A., & Stahle, D. W. (2007). North American drought: Reconstructions, causes, and consequences. *Earth-Science Reviews*, 81(1–2), 93–134. <https://doi.org/10.1016/j.earscirev.2006.12.002>



- Cook, E. R., Seager, R., Kushnir, Y., Zang, C., Büntgen, U., Frank, D., et al. (2015). Old world megadroughts and pluvials during the common Era. *Science Advances*, 1(10), e150056. <https://doi.org/10.1126/sciadv.1500561>
- Cordero, R. R., Feron, S., Damiani, A., Carrasco, J., Karas, C., Wang, C., et al. (2024). Extreme fire weather in Chile driven by climate change and El Niño–Southern Oscillation (ENSO). *Scientific Reports*, 14(1), 1974. <https://doi.org/10.1038/s41598-024-52481-x>
- Coumou, D., Lehmann, J., & Beckmann, J. (2015). The weakening summer circulation in the Northern Hemisphere mid-latitudes. *Science*, 348(6232), 324–327. <https://doi.org/10.1126/science.1261768>
- d'Amour, C. B., Wenz, L., Kalkuhl, M., Steckel, J. C., & Creutzig, F. (2016). Teleconnected food supply shocks. *Environmental Research Letters*, 11(3), 035007. <https://doi.org/10.1088/1748-9326/11/3/035007>
- Di Capua, G., Sparrow, S., Kornhuber, K., Rousi, E., Osprey, S., Wallom, D., et al. (2021). Drivers behind the summer 2010 wave train leading to Russian heatwave and Pakistan flooding. *npj Climate and Atmospheric Science*, 4(1), 55. <https://doi.org/10.1038/s41612-021-00211-9>
- Ding, Q., & Wang, B. (2005). Circumglobal teleconnection in the Northern Hemisphere summer. *Journal of Climate*, 18(17), 3483–3505. <https://doi.org/10.1175/JCLI3473.1>
- Ding, Q., Wang, B., Wallace, J. M., & Branstator, G. (2011). Tropical-extratropical teleconnections in boreal summer: Observed interannual variability. *Journal of Climate*, 24(7), 1878–1896. <https://doi.org/10.1175/2011JCLI3621.1>
- Dong, B., Sutton, R. T., Woollings, T., & Hodges, K. (2013). Variability of the North Atlantic summer storm track: Mechanisms and impacts on European climate. *Environmental Research Letters*, 8(3), 34037. <https://doi.org/10.1088/1748-9326/8/3/034037>
- Dorado-Liñán, I., Ayarzagüena, B., Babst, F., Xu, G., Gil, L., Battipaglia, G., et al. (2022). Jet stream position explains regional anomalies in European beech forest productivity and tree growth. *Nature Communications*, 13(1), 2015. <https://doi.org/10.1038/s41467-022-29615-8>
- Esper, J., Duthorn, E., Krusic, P. J., Timonen, M., & Büntgen, U. (2014). Northern European summer temperature variations over the Common Era from integrated tree-ring density records. *Journal of Quaternary Science*, 29(5), 487–494. <https://doi.org/10.1002/jqs.2726>
- Esper, J., Frank, D., Büntgen, U., Verstege, A., Luterbacher, J., & Xoplaki, E. (2007). Long-term drought severity variations in Morocco. *Geophysical Research Letters*, 34(17), L17702. <https://doi.org/10.1029/2007GL030844>
- Esper, J., Frank, D. C., Wilson, R. J. S., & Briffa, K. R. (2005). Effect of scaling and regression on reconstructed temperature amplitude for the past millennium. *Geophysical Research Letters*, 32(7), L021236. <https://doi.org/10.1029/2004GL021236>
- Florida Ngu, F., Kelman, I., Chambers, J., & Ayebe-Karlsson, S. (2021). Correlating heatwaves and relative humidity with suicide (fatal intentional self-harm). *Scientific Reports*, 11(1), 22175. <https://doi.org/10.1038/s41598-021-01448-3>
- Francis, J. A., & Vavrus, S. J. (2015). Evidence for a wavier jet stream in response to rapid Arctic warming. *Environmental Research Letters*, 10(1), 014005. <https://doi.org/10.1088/1748-9326/10/1/014005>
- Freund, M. B., Henley, B. J., Karoly, D. J., McGregor, H. V., Abram, N. J., & Dietmar, D. (2019). Higher frequency of central Pacific El Niño events in recent decades relative to past centuries. *Nature Geoscience*, 12(6), 450–455. <https://doi.org/10.1038/s41561-019-0353-3>
- Gaupp, F., Hall, J., Hochrainer-Stigler, S., & Dadson, S. (2020). Changing risks of simultaneous global breadbasket failure. *Nature Climate Change*, 10(1), 54–57. <https://doi.org/10.1038/s41558-019-0600-z>
- Gergis, J. L., & Fowler, A. M. (2009). A history of ENSO events since A.D. 1525: Implications for future climate change. *Climatic Change*, 92(3–4), 343–387. <https://doi.org/10.1007/s10584-008-9476-z>
- Goddard, L., & Gershunov, A. (2020). Impact of El Niño of weather and climate extremes. In M. J. McPhaden, A. Santoso, & W. Cai (Eds.), *El Niño Southern oscillation in a changing climate*.
- Graham, N. E., & Hughes, M. K. (2007). Reconstructing the mediaeval low stands of Mono Lake, Sierra Nevada, California, USA. *The Holocene*, 17(8), 1197–1210. <https://doi.org/10.1177/0959683607085126>
- Graham, N. E., Hughes, M. K., Ammann, C. M., Cobb, K. M., Hoerling, M. P., Kennett, D. J., et al. (2007). Tropical pacific-mid-latitude teleconnections in medieval times. *Climatic Change*, 83(1–2), 241–285. <https://doi.org/10.1007/s10584-007-9239-2>
- Grams, C. M., Binder, H., Pfahl, S., Piaget, N., & Wernli, H. (2014). Atmospheric processes triggering the central European floods in June 2013. *Natural Hazards and Earth System Sciences*, 14(7), 1691–1702. <https://doi.org/10.5194/nhess-14-1691-2014>
- Hallam, S., Josey, S. A., McCarthy, G. D., & Hirschi, J. J.-M. (2022). A regional (land–ocean) comparison of the seasonal to decadal variability of the Northern Hemisphere jet stream 1871–2011. *Climate Dynamics*, 59(7–8), 1897–1918. <https://doi.org/10.1007/s00382-022-06185-5>
- Harris, I., Osborn, T. J., Jones, P., & Lister, D. (2020). Version 4 of the CRU TS monthly high-resolution gridded multivariate climate dataset. *Scientific Data*, 7(1), 109. <https://doi.org/10.1038/s41597-020-0453-3>
- Haurwitz, M. W., & Brier, G. W. (1981). A critique of the superposed epoch analysis method: Its application to solar-weather relations. *Monthly Weather Review*, 109(10), 2074–2079. [https://doi.org/10.1175/1520-0493\(1981\)109<2074:ACOTSE>2.0.CO;2](https://doi.org/10.1175/1520-0493(1981)109<2074:ACOTSE>2.0.CO;2)
- Hersbach, H., Bell, B., Berrisford, P., Hirahara, S., Horányi, A., Muñoz-Sabater, J., et al. (2020). The ERA5 global reanalysis. *Quarterly Journal of the Royal Meteorological Society*, 146(730), 1999–2049. <https://doi.org/10.1002/qj.3803>
- Hu, H. M., Shen, C. C., Chiang, J. C., Trouet, V., Michel, V., Tsai, H. C., et al. (2022). Split westerlies over Europe in the early little ice age. *Nature Communications*, 13(1), 4898. <https://doi.org/10.1038/s41467-022-32654-w>
- Hu, H. M., Trouet, V., Spötl, C., Tsai, H. C., Chien, W. Y., Sung, W. H., et al. (2022). Tracing westerly wind directions over Europe since the middle Holocene. *Nature Communications*, 13(1), 7866. <https://doi.org/10.1038/s41467-022-34952-9>
- Huang, B., Thorne, P. W., Banzon, V. F., Boyer, T., Chepurin, G., Lawrimore, J. H., et al. (2017). NOAA Extended Reconstructed Sea Surface Temperature (ERSST), version 5 [Dataset]. *NOAA National Centers for Environmental Information*. <https://doi.org/10.7289/V5T72FNM>
- IPCC. (2022). Summary for policymakers. In H. O. Portner, D. C. Roberts, M. Tignor, E. S. Poloczanska, K. Mintenbeck, A. Alegria, et al. (Eds.), *Climate change 2021: The physical science basis. Contribution of working group I to the sixth assessment report of the intergovernmental panel on climate change*.
- Jiménez-Estève, B., Kornhuber, K., & Domeisen, D. I. V. (2022). Heat extremes driven by amplification of phase-locked circumglobal waves forced by topography in an idealized atmospheric model. *Geophysical Research Letters*, 49(21), e2021GL096337. <https://doi.org/10.1029/2021GL096337>
- Kalnay, E., Kanamitsu, K., Joseph, D., Deaven, D., Gandin, L., et al. (1996). The NCEP/NCAR 40-year reanalysis project. *Bulletin of the American Meteorological Society*, 77(3), 437–472. [https://doi.org/10.1175/1520-0477\(1996\)077<0437:TNYRPP>2.0.CO;2](https://doi.org/10.1175/1520-0477(1996)077<0437:TNYRPP>2.0.CO;2)
- Karoly, D. J. (1983). Rossby wave propagation in a barotropic atmosphere. *Dynamics of Atmospheres and Oceans*, 7(2), 111–125. [https://doi.org/10.1016/0377-0265\(83\)90013-1](https://doi.org/10.1016/0377-0265(83)90013-1)
- Khan, N., Nguyen, H. T., Galelli, S., & Cherubini, P. (2022). Tree-ring evidence of increasing drought risks over the past five centuries amidst projected flood intensification in the Kabul River Basin (Afghanistan and Pakistan). *Geophysical Research Letters*, 49(24), e2022GL100703. <https://doi.org/10.1029/2022GL100703>
- Kornhuber, K., Coumou, D., Vogel, E., Lesk, C., Donges, J. F., Lehmann, J., & Horton, R. M. (2020). Amplified Rossby waves enhance risk of concurrent heatwaves in major breadbasket regions. *Nature Climate Change*, 10(1), 48–53. <https://doi.org/10.1038/s41558-019-0637-z>

- Kornhuber, K., Lesk, C., Schleussner, C. F., Jagermeyr, J., Pfleiderer, P., & Horton, R. M. (2023). Risks of synchronized low yields are underestimated in climate and crop model projections. *Nature Communications*, 14(1), 3528. <https://doi.org/10.1038/s41467-023-38906-7>
- Kornhuber, K., Osprey, S., Coumou, D., Petri, S., Petoukhov, V., Rahmstorf, S., & Gray, L. (2019). Extreme weather events in early summer 2018 connected by a recurrent hemispheric wave-7 pattern. *Environmental Research Letters*, 14(5), 054002. <https://doi.org/10.1088/1748-9326/ab13bf>
- Lee, M.-H., Lee, S., Song, H.-J., & Ho, C.-H. (2017). The recent increase in the occurrence of a boreal summer teleconnection and its relationship with temperature extremes. *Journal of Climate*, 30(18), 7493–7504. <https://doi.org/10.1175/JCLI-D-16-0094.1>
- Li, J., Xie, S.-P., Cook, E. R., Morales, M. S., Christie, D. A., Johnson, N. C., et al. (2013). El Niño modulations over the past seven centuries. *Nature Climate Change*, 3(9), 822–826. <https://doi.org/10.1038/nclimate1936>
- Lin, Y. H., Fosu, B., & Ikuyajolu, O. J. (2023). The impact of tropical SST variability on the northern hemisphere circumpolar teleconnection pattern. *Frontiers in Earth Science*, 11. <https://doi.org/10.3389/feart.2023.1033789>
- Liu, Y., Cobb, K. M., Song, H., Li, Q., Li, C. Y., Nakatsuka, T., et al. (2017). Recent enhancement of central Pacific El Niño variability relative to last eight centuries. *Nature Communications*, 8(1), 15386. <https://doi.org/10.1038/ncomms15386>
- Lorenz, E. N. (1956). *Empirical orthogonal functions and statistical weather prediction, science report No. 1, statistical forecasting project*. Massachusetts Institute of Technology, Department of Meteorology, Massachusetts.
- Luo, M., & Lau, N.-C. (2020). Summer heat extremes in northern continents linked to developing ENSO events. *Environmental Research Letters*, 15(7), 074042. <https://doi.org/10.1088/1748-9326/ab7d07>
- Madden, R. A. (2007). Large-scale, free Rossby waves in the atmosphere—an update. *Tellus*, 59(5), 571–590. <https://doi.org/10.1111/j.1600-0870.2007.00257.x>
- Mann, M. E., Rahmstorf, S., Kornhuber, K., Steinman, B. A., Miller, S. K., & Coumou, D. (2017). Influence of anthropogenic climate change on planetary wave resonance and extreme weather events. *Scientific Reports*, 7(1), 45242. <https://doi.org/10.1038/srep45242>
- Maxwell, J. T., Bregy, J. C., Robeson, S. M., Knapp, P. A., Soule, P. T., & Trouet, V. (2021). Recent increases in tropical cyclone precipitation extremes over the US east coast. *Proceedings of the National Academy of Sciences*, 118(41), e2105636118. <https://doi.org/10.1073/pnas.2105636118>
- Moon, W., Kim, B.-M., Yang, G.-H., & Wettlaufer, J.-S. (2022). Wavier jet streams driven by zonally asymmetric surface thermal forcing. *Proceedings of the National Academy of Sciences*, 119(38), e2200890119. <https://doi.org/10.1073/pnas.2200890119>
- Morice, C. P., Kennedy, J. J., Rayner, N. A., & Jones, P. D. (2012). Quantifying uncertainties in global and regional temperature change using an ensemble of observational estimates: The HadCRUT4 dataset. *Journal of Geophysical Research*, 117(D8), D08101. <https://doi.org/10.1029/2011JD017187>
- Nawrotzki, R. J., Schlak, A. M., & Kugler, T. A. (2016). Climate, migration, and the local food security context: Introducing Terra Populus. *Population and Environment*, 38(2), 164–184. <https://doi.org/10.1007/s11111-016-0260-0>
- Nguyen, H. T. T., & Galelli, S. (2018). A linear dynamical systems approach to streamflow reconstruction reveals history of regime shifts in northern Thailand. *Water Resources Research*, 54(3), 2057–2077. <https://doi.org/10.1038/ncomms15386>
- Nguyen, H. T. T., Turner, S. W. D., Buckley, B. M., & Galelli, S. (2020). Coherent streamflow variability in monsoon Asia over the past eight centuries—links to oceanic drivers. *Water Resources Research*, 56(12). <https://doi.org/10.1029/2020WR027883>
- NOAA Climate Prediction Center. (2023). El Niño/Southern Oscillation (ENSO) diagnostic discussion. Retrieved from [https://www.cpc.ncep.noaa.gov/products/analysis\\_monitoring/ensio\\_advisory/ensodisc.shtml](https://www.cpc.ncep.noaa.gov/products/analysis_monitoring/ensio_advisory/ensodisc.shtml)
- Nojarov, P., & Nikolva, M. (2022). Heat waves and forest fires in Bulgaria. *Natural Hazards*, 114(2), 1879–1899. <https://doi.org/10.1007/s11069-022-05451-3>
- Osman, M. B., Coats, S., Das, S. B., & Chellman, N. (2021). North Atlantic jet stream projections in the context of the past 1,250 years. *Proceedings of the National Academy of Sciences*, 118(38), e2104105118. <https://doi.org/10.1073/pnas.2104105118>
- Peters, G. P., Andrew, R. M., Boden, T., Canadell, J. G., Ciais, P., Le Quere, C., et al. (2013). The challenge to keep global warming below 2°C. *Nature Climate Change*, 3(1), 4–6. <https://doi.org/10.1038/nclimate1783>
- Pfleiderer, P., Schleussner, C.-F., Kornhuber, K., & Coumou, D. (2019). Summer weather becomes more persistent in a 2°C world. *Nature Climate Change*, 9, 666–671. <https://doi.org/10.1038/s41558-019-0555-0>
- Puma, M. J., Bose, S., Chon, S. Y., & Cook, B. I. (2014). Assessing the evolving fragility of the global food system. *Environmental Research Letters*, 10(2), 024007. <https://doi.org/10.1088/1748-9326/10/2/024007>
- Rao, M. P., Cook, E. R., Cook, B. I., Anchukaitis, K. J., D'Arrigo, R. D., Krusic, P. J., & LeGrande, A. N. (2019). A double bootstrap approach to superposed epoch analysis to evaluate response uncertainty. *Dendrochronologia*, 55, 119–124. <https://doi.org/10.1016/j.dendro.2019.05.001>
- Rayner, N. A., Parker, D. E., Horton, E. B., Folland, C. K., Alexander, L. V., Rowell, D. P., et al. (2003). Global analyses of sea surface temperature, sea ice, and night marine air temperature since the late nineteenth century. *Journal of Geophysical Research*, 108(D14), 4407. <https://doi.org/10.1029/2002JD002670>
- Rifai, S., Li, S., & Malhi, Y. (2019). Coupling of El Niño events and long-term warming leads to pervasive climate extremes in the terrestrial tropics. *Environmental Research Letters*, 14(10), 105002. <https://doi.org/10.1088/1748-9326/ab402f>
- Robeson, S. M., Maxwell, J. T., & Ficklin, D. L. (2020). Bias correction of paleoclimatic reconstructions: A new look at 1,200+ years of upper Colorado river flow. *Geophysical Research Letters*, 47(1), e2019GL086689. <https://doi.org/10.1029/2019GL086689>
- Rogers, C. D. W., Kornhuber, K., Perkins-Kirkpatrick, S. E., Loikith, P. C., & Singh, D. (2022). Sixfold increase in historical Northern Hemisphere concurrent large heatwaves driven by warming and changing atmospheric circulations. *Journal of Climate*, 35(3), 1063–1078. <https://doi.org/10.1175/JCLI-D-21-0200.1>
- Röthlisberger, M., Pfahl, S., & Martius, O. (2016). Regional-scale jet waviness modulates the occurrence of midlatitude weather extremes. *Geophysical Research Letters*, 43(20), 10910–10997. <https://doi.org/10.1002/2016GL070944>
- Rousi, E., Kornhuber, K., Beobide-Arsuaga, G., Luo, F., & Coumou, D. (2022). Accelerated Western European heatwave trends linked to more-persistent double jets over Eurasia. *Nature Communications*, 13(1), 3851. <https://doi.org/10.1038/s41467-022-31432-y>
- Sarhadi, A., Ausin, M. C., Wiper, M. P., Touma, D., & Diefenbaugh, N. S. (2020). Multidimensional risk in a nonstationary climate: Joint probability of increasingly severe warm and dry conditions. *Science Advances*, 6(11), 39. <https://doi.org/10.1126/sciadv.aau3487>
- Scholten, R. C., Coumou, D., Luo, F., & Veraverbeke, S. (2022). Early snowmelt and polar jet dynamics co-influence recent extreme Siberian fire seasons. *Science*, 378(6623), 1005–1009. <https://doi.org/10.1126/science.abn4419>
- Screen, J. A., & Simmonds, I. (2014). Amplified mid-latitude planetary waves favour particular regional weather extremes. *Nature Climate Change*, 4(8), 704–709. <https://doi.org/10.1038/nclimate2271>
- Seager, R., Graham, N., Herweijer, C., Gordon, A. L., Kushnir, Y., & Cook, E. (2007). Blueprints for medieval hydroclimate. *Quaternary Science Reviews*, 26(19–21), 2322–2336. <https://doi.org/10.1016/j.quascirev.2007.04.020>

- Seager, R., Henderson, N., & Cane, M. (2022). Persistent discrepancies between observed and modeled trends in the tropical Pacific Ocean. *Journal of Climate*, 35(14), 4571–4584. <https://doi.org/10.1175/JCLI-D-21-0648.1>
- Singh, J., Sippel, S., & Fischer, E. M. (2023). Circulation dampened heat extremes intensification over the midwest USA and amplified over Western Europe. *Communications Earth & Environment*, 4(1), 432. <https://doi.org/10.1038/s43247-023-01096-7>
- Sobel, A. H., Lee, C.-Y., Bowen, S. G., Tippet, M. K., Cane, M. A., Clement, A., et al. (2023). Near-term tropical cyclone risk and coupled Earth system model biases. *Proceedings of the National Academy of Sciences*, 120(33), e2209631120. <https://doi.org/10.1073/pnas.2209631120>
- Stambaugh, M. C., Guyette, R. P., McMurtry, E. R., Cook, E. R., Meko, D. M., & Lupo, A. R. (2011). Drought duration and frequency in the U.S. Corn belt during the last millennium (AD 992–2004). *Agricultural and Forest Meteorology*, 151(2), 154–162. <https://doi.org/10.1016/j.agrformet.2010.09.010>
- Teng, H., Leung, R., Branstator, G., Lu, J., & Ding, Q. (2022). Warming pattern over the Northern Hemisphere midlatitudes in boreal summer 1979–2020. *Journal of Climate*, 35(11), 3479–3494. <https://doi.org/10.1175/JCLI-D-21-0437.1>
- Torrence, C., & Compo, G. P. (1998). A practical guide to wavelet analysis. *Bulletin of the American Meteorological Society*, 79(1), 61–78. [https://doi.org/10.1175/1520-0477\(1998\)079<0061:APGTWA>2.0.CO;2](https://doi.org/10.1175/1520-0477(1998)079<0061:APGTWA>2.0.CO;2)
- Touchan, R., Alchukaitis, K. J., Meko, D. M., Kerchouche, D., Slimani, S., Ilmen, R., et al. (2017). Climate controls Ontree growth in the Western Mediterranean. *The Holocene*, 27(10), 1429–1442. <https://doi.org/10.1177/0959683617693901>
- Trouet, V., Babst, F., & Meko, M. (2018). Recent enhanced high-summer North Atlantic Jet variability emerges from three-century context. *Nature Communications*, 9(1), 180. <https://doi.org/10.1038/s41467-017-02699-3>
- Trouet, V., Esper, J., Graham, N. E., Baker, A., Scourse, J. D., & Frank, D. C. (2009). Persistent positive North Atlantic Oscillation mode dominated the medieval climate anomaly. *Science*, 324(5923), 78–80. <https://doi.org/10.1126/science.1166349>
- Trouet, V., & Van Oldenborgh, G. J. (2013). KNMI climate explorer: A web-based research tool for high-resolution paleoclimatology. *Tree-Ring Research*, 69(1), 3–13. <https://doi.org/10.3959/1536-1098-69.1.3>
- Ulbrich, U., Brucher, T., Fink, A. H., Leckebusch, G. C., Kruger, A., & Pinto, J. G. (2003). The central European floods of August 2002: Part 2—Synoptic causes and considerations with respect to climatic change. *Weather*, 58(11), 434–442. <https://doi.org/10.1256/wea.61.03B>
- van der Schrier, G., Barichivich, J., Briffa, K. R., & Jones, P. D. (2013). A scPDSI-based global data set of dry and wet spells for 1901–2009. *Journal of Geophysical Research—Atmospheres*, 118(10), 4025–4048. <https://doi.org/10.1002/jgrd.50355>
- Vautard, R., Cattiaux, J., Happpé, T., Singh, J., Bonnet, R., Cassou, C., et al. (2023). Heat extremes in Western Europe increasing faster than simulated due to atmospheric circulation trends. *Nature Communications*, 14(1), 6803. <https://doi.org/10.1038/s41467-023-42143-3>
- Vitart, F. (2019). Chapter 17 – sub-Seasonal to seasonal prediction of weather extremes. In: The gap between weather and climate forecasting, 365–386. In M. J. McPhaden, A. Santoso, & W. Cai (Eds.), *El Niño southern oscillation in a changing climate*.
- Wahl, E. R., Zorita, E., Trouet, V., & Taylor, A. H. (2019). Jet stream dynamics, hydroclimate, and fire in California from 1600 CE to present. *Proceedings of the National Academy of Sciences*, 116(12), 5393–5398. <https://doi.org/10.1073/pnas.1815292116>
- Wang, H., Wang, B., Huang, F., Ding, Q., & Lee, J.-Y. (2012). Interdecadal change of the boreal summer circumglobal teleconnection (1958–2010). *Geophysical Research Letters*, 39(12), e2012GL052371. <https://doi.org/10.1029/2012GL052371>
- Wang, Y., Hu, K., Huang, G., & Tao, W. (2021). Asymmetric impacts of El Niño and La Niña on the Pacific–North American teleconnection pattern: The role of subtropical jet stream. *Environmental Research Letters*, 16(11), 114040. <https://doi.org/10.1088/1748-9326/ac31ed>
- Wang, Z., Zhang, G., Dunkerton, T. J., & Jin, F.-F. (2020). Summertime stationary waves integrate tropical and extratropical impacts on tropical cyclone activity. *Proceedings of the National Academy of Sciences*, 117(37), 22720–22726. <https://doi.org/10.1073/pnas.2010547117>
- Wei, W., Yan, Z., & Li, Z. (2021). Influence of Pacific decadal oscillation on global precipitation extremes. *Environmental Research Letters*, 16(4), 044031. <https://doi.org/10.1088/1748-9326/abed7c>
- Wells, N., Goddard, S., & Hayes, M. J. (2004). A self-calibrating palmer drought severity index. *Journal of Climate*, 17(12), 2335–2351. [https://doi.org/10.1175/1520-0442\(2004\)017<2335:ASPDSEI>2.0.CO;2](https://doi.org/10.1175/1520-0442(2004)017<2335:ASPDSEI>2.0.CO;2)
- White, R. H., Kornhuber, K., Martius, O., & Wirth, V. (2022). From atmospheric waves to heatwaves: A waveguide perspective for understanding and predicting concurrent, persistent, and extreme extratropical weather. *Bulletin of the American Meteorological Society*, 103(3), 923–935. <https://doi.org/10.1175/BAMS-D-21-0170.1>
- Wicker, W., Harnik, N., Pyrina, M., & Domeisen, D. I. (2024). Heatwave location changes in relation to Rossby wave phase speed. *Geophysical Research Letters*, 51(14), e2024GL108159. <https://doi.org/10.1029/2024GL108159>
- Wilks, D. S. (2016). The stippling shows statistically significant grid points: How research results are routinely overstated and over interpreted, and what to do about it. *Bulletin of the American Meteorological Society*, 97(12), 2263–2273. <https://doi.org/10.1175/BAMS-D-15-00267.1>
- Wills, R. C. J., Dong, Y., Proistosescu, C., Armour, K. C., & Battisti, D. S. (2022). Systematic climate model biases in the large-scale patterns of recent sea-surface temperature and sea-level pressure change. *Geophysical Research Letters*, 49(17), e2022GL100011. <https://doi.org/10.1029/2022GL100011>
- Woollings, T., & Blackburn, M. (2012). The North Atlantic jet stream under climate change and its relation to the NAO and EA patterns. *Journal of Climate*, 25(3), 886–902. <https://doi.org/10.1175/JCLI-D-11-00087.1>
- Woollings, T., Drouard, M., O'Reilly, C. H., Sexton, D. M. H., & McSweeney, C. (2023). Trends in the atmospheric jet streams are emerging in observations and could be linked to tropical warming. *Communications Earth & Environment*, 4(1), 125. <https://doi.org/10.1038/s43247-023-00792-8>
- World Meteorological Organization. (2023). Exceptional heat and rain, wildfires, and floods mark summer of extremes. Retrieved from <https://public.wmo.int/en/media/news/exceptional-heat-and-rain-wildfires-and-floods-mark-summer-of-extremes>
- World Weather Attribution. (2023). Extreme heat in North America, Europe and China in July 2023 made much more likely by climate change. Retrieved from <https://www.worldweatherattribution.org/extreme-heat-in-north-america-europe-and-china-in-july-2023-made-much-more-likely-by-climate-change/>
- Xu, G., Broadman, E., Dorado-Linan, F., Klippel, L., Meko, M., Büntgen, U., et al. (2024). Jet stream driven European climate extremes and agricultural productivity since 1300 CE. *Nature*, 634(8034), 600–608. <https://doi.org/10.1038/s41586-024-07985-x>
- Yang, X., Zeng, G., Zhang, S., Iyakaremye, V., Shen, C., Wang, W. C., & Chen, D. (2024). Phase-locked Rossby wave-4 pattern dominates the 2022-like concurrent heat extremes across the Northern Hemisphere. *Geophysical Research Letters*, 51(4), e2023GL107106. <https://doi.org/10.1029/2023GL107106>
- Yasui, S., & Watanabe, M. (2010). Forcing processes of the summertime circumglobal teleconnection pattern in a dry AGCM. *Journal of Climate*, 23(8), 2093–2114. <https://doi.org/10.1175/2009JCLI3323.1>
- Zhang, K., Chen, T.-H., & Begley, C. E. (2015). Impact of the 2011 heat wave on mortality and emergency department visits. *Environmental Health*, 14(1), 11. <https://doi.org/10.1186/1476-069X-14-11>
- Zhou, Z., Zhang, L., Zhang, Q., Hu, C., Wang, G., She, D., & Chen, J. (2024). Global increase in future compound heat stress-heavy precipitation hazards and associated socio-ecosystem risks. *npj Climate and Atmospheric Science*, 7(1), 33. <https://doi.org/10.1038/s41612-024-00579-4>

## References From the Supporting Information

- Brooke, J. (1984). Heat wave stall over city; 4 more die. <https://www.nytimes.com/1984/06/12/nyregion/heat-wave-stall-over-city-4-more-die.html>
- Burt, C. C. (2013). *Update 7/24: Heat wave continues in Siberia*. Wunderground – Wunderblog Archive. Retrieved from <https://www.wunderground.com/blog/weatherhistorian/update-724-heat-wave-continues-in-siberia.html>
- Cai, J., Zhang, S., Zhang, Y., Mengkui, L., Wei, Y., & Xie, P. (2022). Characteristics and cause analysis of the 1954 Yangtze precipitation anomalies. *Remote Sensing*, 14(3), 555. <https://doi.org/10.3390/rs14030555>
- Hannaford, J., Lloyd-Hughes, B., Keef, C., Parry, S., & Prudhomme, C. (2011). Examining the large-scale spatial coherence of European drought using regional indicators of precipitation and streamflow deficit. *Hydrological Processes*, 25(7), 1146–1162. <https://doi.org/10.1002/hyp.7725>
- Hisdal, H., Stahl, K., Tallaksen, L. M., & Demuth, S. (2001). Have streamflow droughts in Europe become more severe or frequent? *International Journal of Climatology*, 21(3), 317–333. <https://doi.org/10.1002/joc.619>
- Karl, T. R., & Quayle, R. G. (1981). The 1980 summer heat wave and drought in historical perspective. *Monthly Weather Review*, 109(10), 2055–2073. [https://doi.org/10.1175/1520-0493\(1981\)109<2055:TSHWAD>2.0.CO;2](https://doi.org/10.1175/1520-0493(1981)109<2055:TSHWAD>2.0.CO;2)
- Kysely, J. (2004). Mortality and displaced mortality during heat waves in the Czech Republic. *International Journal of Biometeorology*, 49(2), 91–97. <https://doi.org/10.1007/s00484-004-0218-2>
- Meshcherskaya, A. V., & Blazhevich, V. G. (1997). The drought and excessive moisture indices in a historical perspective in the principal grain-producing regions of the former Soviet union. *Journal of Climate*, 10, 2670–2682. [https://doi.org/10.1175/1520-0442\(1997\)010<2670:TDAEMI>2.0.CO;2](https://doi.org/10.1175/1520-0442(1997)010<2670:TDAEMI>2.0.CO;2)
- Nace, R. L., & Pluhowski, E. J. (1965). *Drought of the 1950's with special reference to the mid-continent*. U.S. Government Printing Office.
- National Weather Service. (2023). Top ten heat events. Retrieved from <https://www.weather.gov/lmk/top10heat>. Accessed July 5, 2023.
- New York Times. (1996). 8-day heat wave claims 20 victims in Texas and Oklahoma.
- National Oceanic and Atmospheric Administration. (2023). Heavy rains inundate St. Petersburg – Fact Sheet. Retrieved from <https://www.weather.gov/media/tbw/paig/PresAmFlood1979.pdf>. Accessed July 5, 2023.
- Parry, S., Hannaford, J., Lloyd-Hughes, B., & Prudhomme, C. (2012). Multi-year droughts in Europe: Analysis of development and causes. *Hydrological Research*, 43(5), 689–706. <https://doi.org/10.2166/nh.2012.024>
- Puckett, K. (2014). 1964 flood: Worst flood in Montana's history left death, destruction. *Great Falls Tribune*, May 25, 2014. <https://eu.greatfallstribune.com/story/news/local/2014/05/25/50th-anniversary-1964-flood/9563135/>
- Rannie, W. F. (1980). The Red River flood control system and recent flood events. *Journal of the American Water Resources Association*, 16(2), 207–214. <https://doi.org/10.1111/j.1752-1688.1980.tb02380.x>
- Rostvedt, J. O. (1971). *Summary of floods in the United States during 1966*. US Geological Survey Water Supply Paper 1970.
- Santos, M. J., Verissimo, R., Fernandes, S., Orlando, M., & Rodrigues, R. (2000). *Overview of meteorological drought analysis on Western Europe*. ARIDE Technical Report 10. Water Institute.
- Sheffield, J., Andreadis, K. M., Wood, E. F., & Lettenmaier, D. P. (2009). Global and continental drought in the second half of the twentieth century: Severity-area-duration analysis and temporal variability of large scale events. *Journal of Climate*, 22(8), 1962–1981. <https://doi.org/10.1175/2008JCLI2722.1>
- Shehata, M., & Mizunaga, H. (2018). Flash flood risk assessment for Kyushu Island, Japan. *Environmental Earth Sciences*, 77(3), 76. <https://doi.org/10.1007/s12665-018-7250-8>
- Singh, D., Horton, D. E., Tsiang, M., Haugen, M., Ashfaq, M., Mei, R., et al. (2014). Severe precipitation in northern India in June 2013: Causes, historical context, and changes in probability. *Bulletin of the American Meteorological Society*, 95(9), S58–S60.
- Teufel, B., Diro, G. T., Whan, K., Sushama, L., Jeong, D. I., Ganji, A., et al. (2017). Investigation of the 2013 Alberta flood from weather and climate perspectives. *Climate Dynamics*, 48(9–10), 2881–2899. <https://doi.org/10.1007/s00382-016-3239-8>
- Twardosz, R., & Kosowska-Cezak, U. (2013). Exceptionally hot summers in central and Eastern Europe (1951–2010). *Theoretical and Applied Climatology*, 112(3–4), 617–628. <https://doi.org/10.1007/s00704-012-0757-0>
- Trenberth, K. E., & Guillemot, C. J. (1996). Physical processes involved in the 1988 drought and the 1993 floods in North America. *Journal of Climate*, 9(6), 1288–1298. [https://doi.org/10.1175/1520-0442\(1996\)009<1288:PPIITD>2.0.CO;2](https://doi.org/10.1175/1520-0442(1996)009<1288:PPIITD>2.0.CO;2)
- United Nations Department of Humanitarian Affairs. (1991). China – Floods Jun 1991 UNDRO situation reports 1-9. UNDRO 91/1045. Retrieved from <https://reliefweb.int/report/china/china-floods-jun-1991-undro-situation-reports-1-9>
- Veryard, R. G. (1956). Looking back on 1955. *Weather*, 11(3), 83–88. <https://doi.org/10.1002/j.1477-8696.1956.tb00296.x>
- Xia, J., Tu, K., Yan, Z., & Qi, Y. (2016). The super-heat wave in eastern China during July–August 2013: A perspective of climate change. *International Journal of Climatology*, 36(3), 1291–1298. <https://doi.org/10.1002/joc.4424>
- Xue, Z., & Ullrich, P. (2021). A retrospective and prospective examination of the 1960s U.S. Northeast drought. *Earth's Future*, 9(7), e2020EF001930. <https://doi.org/10.1029/2020EF001930>
- Ye, Q., & Glantz, M. H. (2005). The 1998 Yangtze floods: The use of short-term forecasts in the context of seasonal to interannual water resource management. *Mitigation and Adaptation Strategies for Global Change*, 10(1), 159–182. <https://doi.org/10.1007/s11027-005-7838-7>
- Zaidman, M. D., Rees, H. G., & Young, A. R. (2001). Spatio-temporal development of streamflow droughts in north-west Europe. *Hydrology and Earth System Sciences*, 5(4), 733–751. <https://doi.org/10.5194/hess-6-733-2002>